Journal of Energetic Materials
Publication details, including instructions for authors and subscription information:
http://www.informaworld.com/smpp/title~content=t713770432

Influence of Pressing Intensity on the Microstructure of PBX 9501

P. D. Peterson; M. A. Fletcher; E. L. Roemer

Online publication date: 18 June 2010

To cite this Article Peterson, P. D. , Fletcher, M. A. and Roemer, E. L.(2003) 'Influence of Pressing Intensity on the Microstructure of PBX 9501', Journal of Energetic Materials, 21: 4, 247 — 260
To link to this Article: DOI: 10.1080/713770436
URL: http://dx.doi.org/10.1080/713770436

Energetic Materials, 21: 247–260, 2003

ISSN: 0737-0652 print
DOI: 10.1080/07370650390274566

Taylor & Francis
Taylor & Francis Group

Influence of Pressing Intensity on the Microstructure of PBX 9501

P. D. PETERSON
M. A. FLETCHER
E. L. ROEMER

High Explosives Science and Technology,
Los Alamos National Laboratory,
Los Alamos, NM, USA

Microstructural features, such as defects, crystal morphology, and crystal size distribution, can significantly affect the ignition sensitivity, performance, and mechanical properties of energetic materials. To evaluate the influence of pressing parameters on microstructure, three cylinders of PBX 9501 were pressed at 5,000, 15,000, and 30,000 psi, using a 100 ton heated steel die press. Polarized light microscopy images taken at 144 locations within each cylinder show differences in porosity, crystal size, and crystal size distribution between cylinders and at different locations within the same cylinder. Scanning electron microscopy further verifies increased fracture and pulverization of HMX crystals during pressing.

Keywords: PBX 9501, pressing parameters, particle site, microscopy

Introduction

Studies have shown that the final density distribution in die-pressed inert powders can be dramatically affected by variations in a number of variables, including initial particle size, morphology, and size distribution [1–5], pressing intensity [3], pressing temperature [6],

Address correspondence to P. D. Peterson, High Explosives Science and Technology, Los Alamos National Laboratory, Los Alamos, NM 87545 USA. E-mail: pdp@lanl.gov

number of pressure cycles [1,7], die wall lubrication [2,3,5,7], and shape/aspect ratio of the final pressed part [1,3,5,7].

In the preparation of consolidated charges of high explosive, these same pressing parameters are often varied to account for lot-to-lot differences in molding powder. For example, PBX 9501 is a high-explosive formulation composed of 94.9/2.5/2.5/0.1 wt% HMX (3:1 mass ratio of Class 1 (coarse) and Class 2 (fine))/Estane/a eutectic mixture of bis(2,2 dinitropropyl) acetal and bis (2,2-dinitropropyl) formal (abbreviated BDNPA-F)/and Irganox (a free-radical inhibitor). Sieve-size specifications for class 1 and 2 HMX are specified by MIL-DTL-45444C. However, because this specification is broad enough to allow for some lot-to-lot differences in the size and distribution of both the coarse and fine HMX constituents, variables such as ultimate pressure, pressing temperature, number of pressing cycles, dwell time, and/or rest time (between cycles) must be varied between lots to achieve the nominal bulk density of 1.830 g/cc [8]. Although the nominal bulk density is met, variations in pressing parameters will consequently lead to differences in average crystal size between samples and in crystal size distribution and density gradients across a given sample. In addition, microstructural features, such as crystal morphology, crystal size distribution, and density gradients, have been shown to contribute significantly to PBX 9501 mechanical properties [8,9], ignition sensitivity [10,11], and performance [12–14]. Therefore, understanding how differences in pressing intensity and other pressing parameters affect crystal size distributions and density gradients within PBX 9501 is essential to the construction of full-scale constitutive models for both the pristine and damaged materials.

To begin to understand the influence of pressing variations on microstructure, this article examines the effect of pressing intensity on the crystal morphology, crystal size distribution, and density gradients within pressed cylinders of PBX 9501.

Experimental Procedure

Materials

To evaluate the effect of pressing intensity on the microstructure of PBX 9501, three cylinders ($1'$ $\phi \times 1''$ long ($L/d = 1$)) of Lot HOL89C730-010 (manufactured by Holston Army Ammunition Plant) have been pressed at 5,000, 15,000, and 30,000 psi, respectively, using a 100 ton heated steel die press. Each specimen was pressed at 90 °C, under vacuum, for two 3-minute cycles, with a 3 minute rest

period between cycles. Temperature was maintained during the rest period. The vacuum pulled was 200 µm for each specimen during pressing. Zinc stearate mold release was generously applied to all parts of the die prior to loading the molding powder for each specimen.

Methods

Polarized light microscopy (PLM) and scanning electron microscopy (SEM) techniques were used to examine the microstructure between specimens and at locations within the same specimen. In addition, the pressed specimens' crystal size and distributions were compared to the sieve distributions for the original 3:1 HMX distribution [15] and to the pristine molding powder for HOL Lot 89C730-010 (which consists of agglomerates of HMX and binder called prills).

Specimen Preparation and Analysis

To prepare the samples for PLM analysis and density measurement, two cross-sections were cut from each cylinder and then sectioned as shown in Figure 1. Cutting and sectioning of the pressed specimens was done remotely using a 125 mm aluminum oxide cut-off wheel at

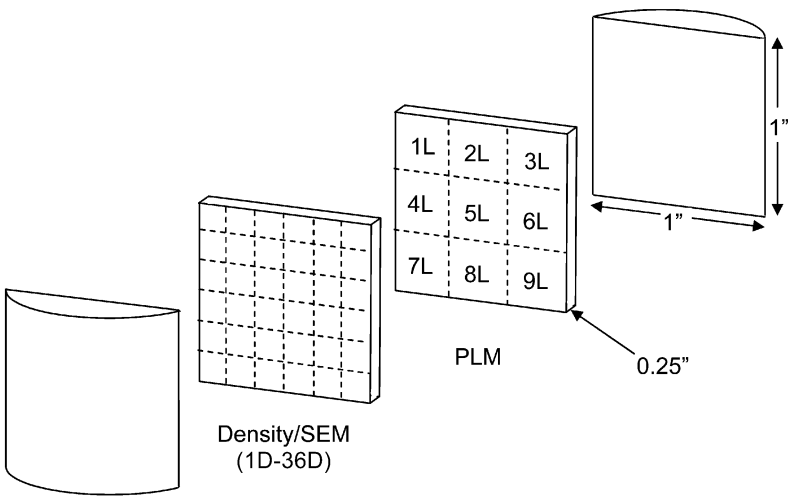

Figure 1. Sectioning of PBX 9501 specimens.

1000 rpm and a feed rate of 0.035 mm/sec. Specimens 1L–9L were each potted separately in Struers Epofix two-part epoxy under vacuum (500 mbar) and allowed to set overnight under nitrogen at 500 psi. The faces of interest were then polished remotely using 1200, 2400, and 4000 grit SiC papers, and 1 and 0.3 μm Al_2O_3 polishing powders on a Struers Rotopol-25/Pedemin˙S automatic grinding-polishing machine. A final polishing was done by hand using an OP-S suspension (0.03 μm). Molding powder was potted and polished using the same technique.

Specimens 1L–9L were then examined using a Lieca DM-RXA PLM. The microscope is equipped with a Diagnostic Instruments SPOT 100 camera that provides 1315×1033 pixels digital micrographs. All PLM images were taken with parallel polarizers in reflectance mode. A total of 16 images were taken at a magnification of 50× across each of the nine subsections of each sample. These 50× images encompassed the entire sample. Binder rich areas were selected from each subsection and imaged at 200×. A total of 864 images were taken and analyzed across the three specimens. An image processing and analysis routine was written using Clemex Vision^{TM} image analysis software. This routine incorporates image processing, color thresholding, and geometric constraints to differentiate and label HMX crystals, binder, and voids. Area percentages, average crystal sizes, and crystal size distributions were then determined as a function of pressing intensity and position within the sample.

A brief synopsis of the routine follows. An initial black top hat filter was first applied to each image to highlight and label small, dark areas within the image as voids. A high-level sharpening filter was then applied to the original image to increase the absolute intensity difference between the HMX crystals and the darker binder, followed by a single cycle smoothing filter using a 3 pixel×3 pixel kernel. The smoothing filter eliminates extraneous noise produced in the image during sharpening. Following the smoothing filter, a lower-level sharpening filter was applied to the image to enhance further crystal-binder intensity differences. HMX crystals were then identified by their gray-level intensity threshold and labeled using a colored bitplane. To separate contacting crystals while maintaining each crystal's original size, a series of successive erosion and dilation filters were then applied to the colored HMX bitplane, and any features in the image that were not part of the HMX or void bitplanes were necessarily assumed to be binder. Crystals, binder, and voids were then labeled using colored

bitplanes. In every case the colored bitplanes were visually inspected against the original image as a reality check. Area percentages, average crystal sizes, and crystal size distributions were then calculated from the respective bitplanes.

Immersion density measurements were taken for 36 subsections across each sample (1D-36D; see Figure 1). In addition, the binder was stripped from the four centermost density pieces using methyl ethyl ketone (MEK). In each case, prior to adding the PBX 9501 specimens the MEK was saturated with a 3:1 mass ratio of class 1 and 2 HMX to prevent dissolution of HMX from the pressed specimens. During the stripping process, the samples were placed in a shaker for 30 minutes at 250 rpm and then centrifuged for 10 minutes at 2500 rpm. The MEK was then siphoned off using a pipet and the crystals were rinsed, first with HMX saturated ethanol and then with water to remove any excess MEK. After drying overnight, the crystals were analyzed using a Leo 1525 Field Emission Scanning Electron Microscopy (FESEM).

Results and Discussion

Typical postanalysis PLM images at 50× and 200× are shown in Figure 2. The crystals, binder, and voids have been labeled white, gray, and black, respectively. The images clearly show several crystals that have fractured either during processing of the molding powder or during pressing of the final high explosive. Fracture of the HMX crystals may also have occurred when the specimens were sectioned with the aluminum oxide cut-off wheel, but it is believed that sufficient material is removed from the specimen during polishing to eliminate any residual effects due to the sectioning method. In either case, as all specimens were sectioned and polished using the same methods, so differences between specimens can be attributed only to variations in pressing intensity.

Similar images were analyzed from 144 locations (at 50× and 200× magnifications) across each pressing sample to determine local and bulk average crystal sizes and crystal size distributions. 50× images covered the entire sample face and were used to analyze crystals larger than $35\,\mu^2$. Crystal size distributions and percentages for crystals between $4\,\mu^2$ and $35\,\mu^2$ were determined from the 200× images. Percentages and size distributions were then calculated by normalizing the 200× image data to the area of its corresponding 50× image.

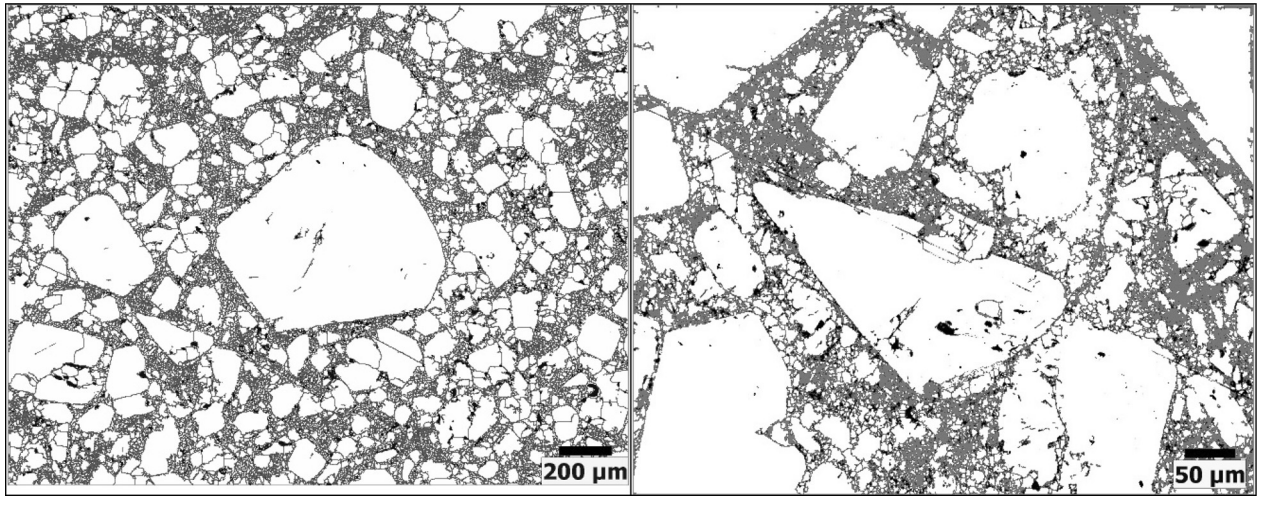

Figure 2. Postanalysis image (location near bottom of 15,000 psi specimen) at 50× (left, bar = 200 µm) and 200× (right, bar = 50 µm). White = crystals, gray = binder, black = void.

Average crystal sizes were determined for pristine HMX from HOL89C730-010, the PBX 9501 molding powder, and each of the three pressed PBX 9501 specimens. Average crystal size for the pristine HMX was calculated from sieve analysis data for the 3:1 blend [15]. Average crystal sizes for the molding powder and pressed specimens were determined from image analysis. In image analysis the necessary assumption is that all crystals are sliced, polished, and imaged along their volumetric centroid. Crystals that have not been imaged along their centroid will appear to have reduced crystal sizes. As a consequence, average particle sizes measured with microscopy will be underestimated, and apparent particle size distributions will be shifted toward smaller values. The possible magnitude of this error will increase with particle size as the probability of slicing the particle through its centroid decreases. Fortunately the overall number of large particles is also statistically small.

Average crystal sizes from the PLM analysis are as follows:

Pristine 3:1 blend of HMX[2]	132.2 μm^2
Molding powder	45.7 μm^2
5 ksi	24.3 μm^2
15 ksi	21.6 μm^2
30 ksi	19.7 μm^2

Crystal size was found to decrease as pressing intensity is increased, in agreement with [16]. Contour plots of the average crystal size across each specimen clearly show that crystal size differs both within and between pressing samples (Figure 3). Near the center of the 5,000 psi specimen a semiprotected area is clearly seen, with remnants still visible at 15,000 and 30,000 psi. The semiprotected area indicates that a majority of the crystal fracture during pressing occurs along the top, bottom, and circumferential edges of the cylinders, where the effects of die and wall friction are greatest.

Comparison of immersion density profiles with the crystal size profiles indicates that areas of large crystal size correspond to areas of low density (Figure 3). Neither the crystal size contours nor the density contours are axisymmetric, presumably due to local variations in the initial molding powder packing. Similar density contours have been suggested for die pressed powders with aspect ratios of $L/d = 1$

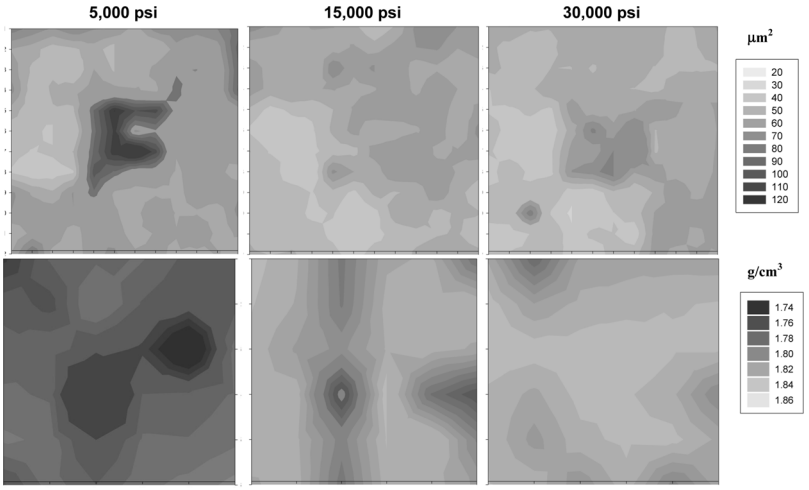

Figure 3. Average crystal size (above) and density contours (below) across the entire ($1'' \times 1''$) sample for three pressing intensities. Die pressed up from bottom.

under cyclic loading [1,2,7]. Very different density distributions have been shown to exist within statically pressed PBX 9501 [17]. Comparison of average crystal size profiles and pressed density profiles along the center axis of the pressed cylinder indicates that the inverse correlation between the two is particularly strong away from the top and bottom edges of the cylinder where the effects of friction are minimized (Figure 4). Near the top and bottom faces of the cylinder, frictional effects lead to a slight decrease in crystal size and an increase in density.

Overall size distributions for each of the three pressed specimens have been measured and compared with size distributions for molding powder and with the original HMX size distribution as determined from sieve analysis (Figure 5). The dip at approximately $2000\,\mu m^2$ in the pressed samples and $6000\,\mu m^2$ in the molding powder and sieve data are characteristics of a bimodal crystal size distribution. The shift in the location of the dip further signifies that fracture and pulverization are occurring during pressing. The decrease in the fraction of crystals of size 100–2000 μm^2 between pressing specimens indicates fracture occurs in many of these crystals as pressing intensity increases. An increase in the fraction of crystals smaller than $100\,\mu m^2$can also be seen across the three pressed specimens, further

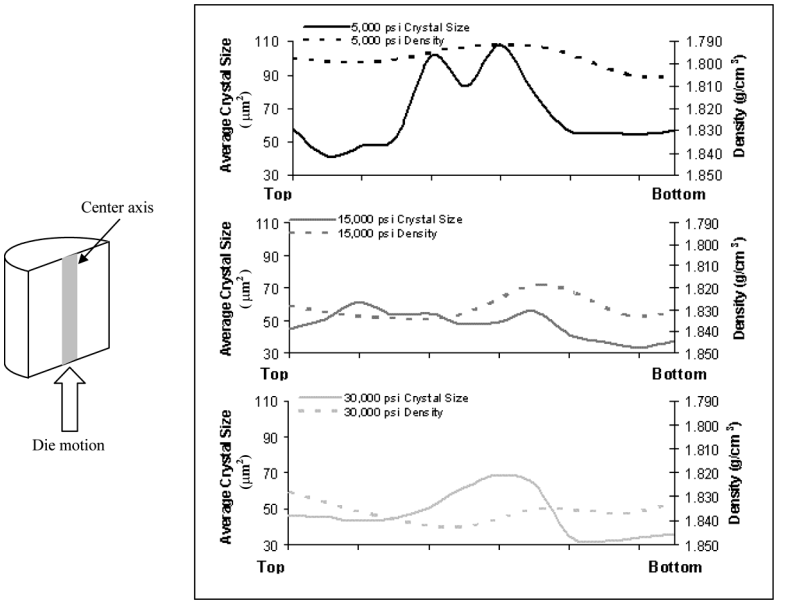

Figure 4. Comparison of average crystal size and density along the center line of pressed PBX 9501 cylinders.

indicating the generation of small crystals as more fracture and pulverization occurs due to crystal-crystal contact. Overall, more than a seven-fold increase in the number of crystals/in^2 occurs as the original molding powder is pressed to 30,000 psi.

Crystal size distributions were also compared for positions 1–3 (top third of the cylinder), 4–6 (center third of the cylinder), and 7–9 (bottom third of the cylinder) within the same pressed cylinder. The results are shown in Figure 6 for the 5,000, 15,000, and 30,000 psi specimens respectively. For all three pressed cylinders, image analysis indicates the greatest number of crystals exist along the bottom of the pressed cylinder near the impinging die (positions 7–9). Positions 4–6 (the middle of the cylinder) contain the least number of crystals, which further indicates that this region is at least partially protected during die compaction. The top third of the cylinder (positions 1–3) demonstrates intermediate numbers of crystals. These crystal size distributions further suggest that crystal fracture and pulverization are strongly related to die and wall friction.

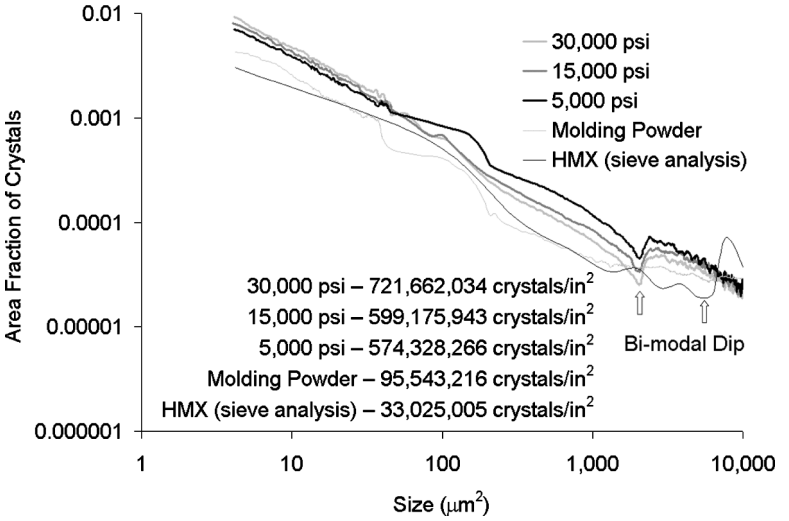

Figure 5. Crystal size distributions of entire pressed specimens compared to molding powder and sieve analysis of original 3:1 HMX distribution.

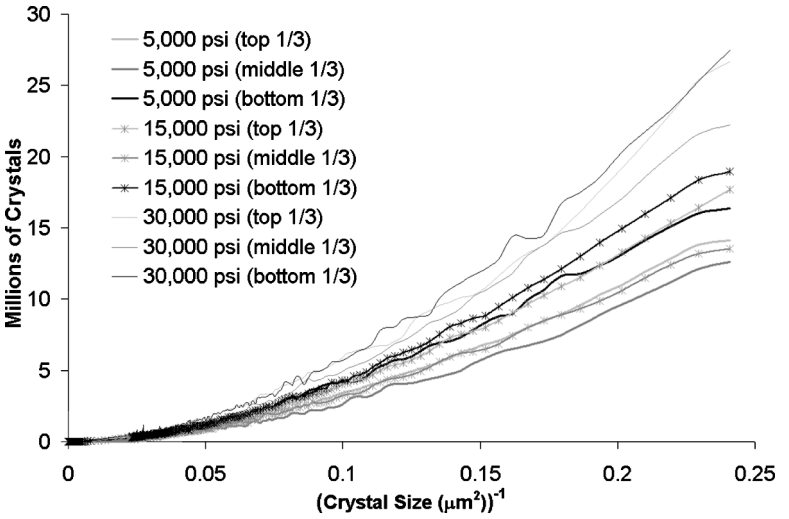

Figure 6. Crystal size distribution within pressed specimens.

Representative FESEM images of crystals extracted from the molding powder, and crystals extracted from the center of the

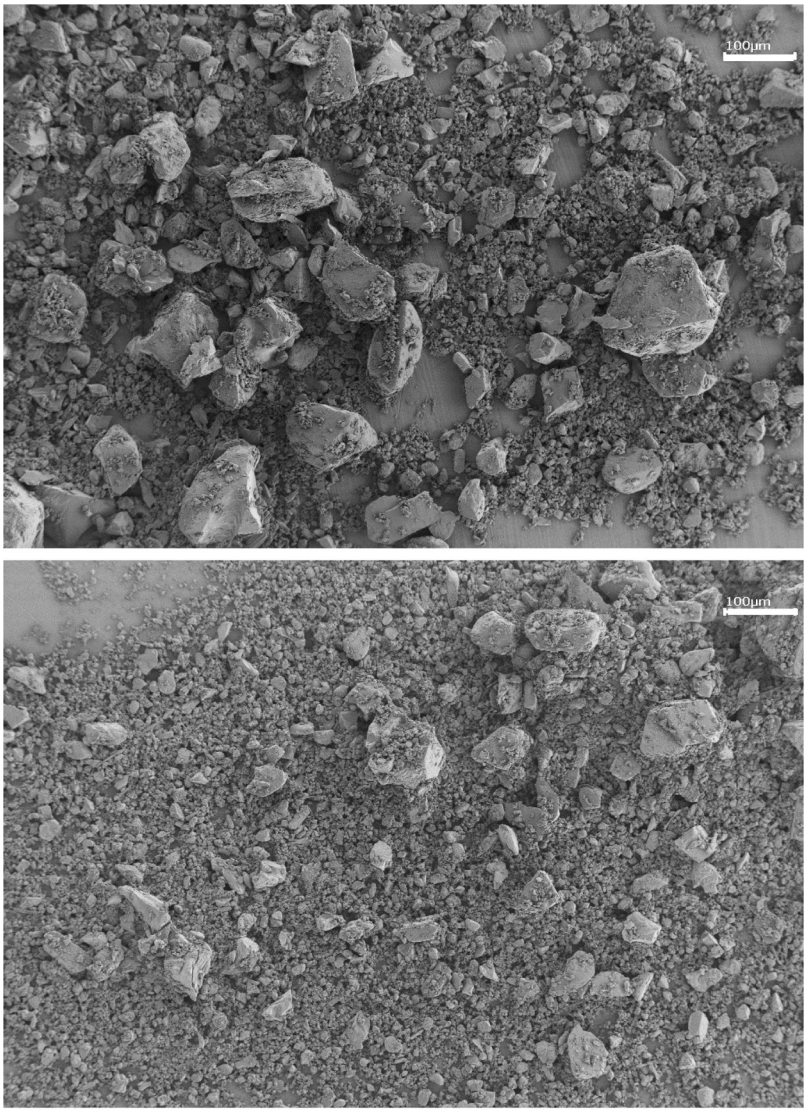

Figure 7. FESEM images (molding prills—top, 30,000 psi—bottom). Bar = 100 µm.

30,000 psi specimen, clearly show increased crystal fracture has occurred during pressing (Figure 7). Crystals extracted from molding powder show multiple fractures and damaged crystal faces. Crystals

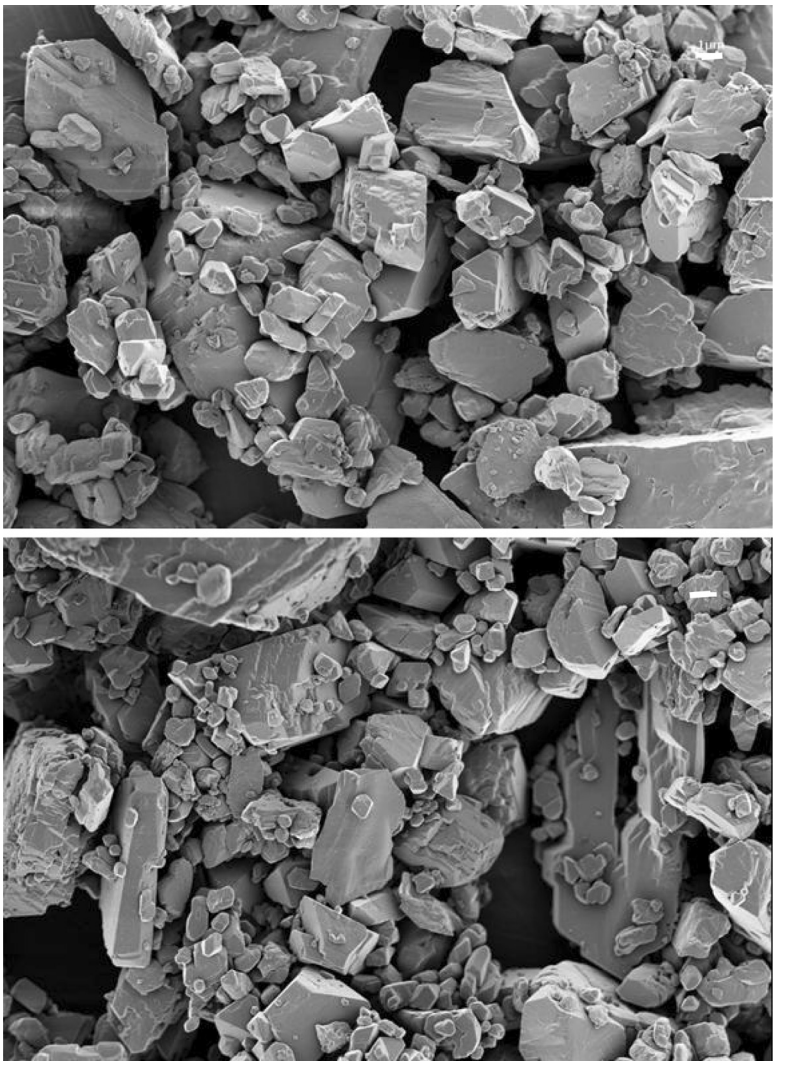

Figure 8. Higher-magnification FESEM images of the smaller HMX crystals (molding prills—top, 30,000 psi—bottom). Bar = 1 μm.

extracted from the center of the 30,000 psi specimen show severe damage to both crystal edges and faces. Higher magnification images show that many of the crystals have been fractured and pulverized until they have become spherical particles with diameters approaching 1 μm (Figure 8). Interestingly, very few crystals with diameters smaller than 1 μm are seen, indicating that there may be a limiting size for crystal fragmentation at these pressures. The size limit could also result from preferential chemical dissolution of the smallest crystals in the MEK or Ethanol during the binder stripping process. However, as both solutions were saturated with HMX and as a few very small crystals are visible, we believe the limiting size to be a function of the pressing.

Conclusions

Differences in pressing intensity can lead to significant variations in crystal size distribution between samples, and in average crystal size and crystal size distribution variations within pressed cylinders of PBX 9501. A majority of the crystal fracture and material consolidation during pressing occurs along the top, bottom, and edges of the cylinder. Near the center of a pressed cylinder, a partially protected area exists where crystal fracture is minimized during pressing. At higher pressing intensities, the fraction of crystals smaller than $100\,\mu m^2$ in PBX 9501 increases dramatically as the crystal-crystal contact further fractures and pulverizes the HMX. However, a limiting crystal size may exist for fragmentation of the HMX crystals at these pressures.

Acknowledgments

The authors would like to thank Stephanie Hagelberg and Bart Olinger for immersion density measurements, and Anna Giambra for HMX crystal preparations.

References

[1] Fu, Y., G. Jiang, J. J. Lannutti, R. H. Wagoner, and G. S. Daehn. 2002. Effect of cyclic pressure consolidation on the uniformity of metal matrix composites. *Metal. and Mat. Trans. A* 33A: 183.

[2] Long, W. M. 1960. Radial pressures in powder compaction. *Powder Metallurgy* 6: 73.

[3] Thompson, R. A. 1981. Mechanics of powder pressing: I. model for powder densification. *Ceramic Bulletin* 60(2): 237.
[4] Shotton, E., and D. Ganderton. 1961. The strength of compressed tablets. *Journal of Pharmacy and Pharmacology* 13(S): T144.
[5] MacLeod, H. M, and K. Marshall. 1977. The determination of density distributions in ceramic compacts using autoradiography. *Powder Technology* 16: 107.
[6] Bocchini, G. F. 1999. Warm compaction of metal powders: why it works, why it requires a sophisticated engineering approach. *Powder Metallurgy* 42(2): 171.
[7] Jiang, G., G. S. Daehn, J. J. Lannutti, Y. Fu, and R. H. Wagoner. 2001. Effects of lubrication and aspect ratio on the consolidation of metal matrix composites under cyclic pressure. *Acta Materialia* 49: 1471.
[8] Meyer, T. M., R. V. Browing, and R. Spence. 2000. Compression properties of PBX 9501 at densities from 1.60 to 1.83 g/cc. Pantex Plant report, DOE/AL/65030–00–04, February.
[9] Thompson, D. G, and W. J. Wright. 2003. Mechanical properties from PBX 9501 pressing study. Presented at the 13th American Physical Society Topical Conference on Shock Compression of Condensed Matter, Portland, OR.
[10] Simpson, R. L. et al. 1989. Particle size effects in the initiation of explosive containing reactive and non-reactive continuous phases. In *Proc. 9th Intl. Detonation Symp.*, p. 25.
[11] Howe, P. M. 1998. Trends in the shock initiation of heterogeneous explosives. In *Proc. 11th Intl. Detonation Symp* p. 670.
[12] Dick, J. J. 1983. Measurement of the shock initiation of low-density HMX. *Combustion and Flame* 54(1–3): 121.
[13] Skidmore, C. B. et al. 1998. The evolution of microstructural changes in pressed HMX explosives. In *Proc. 11th Intl. Detonation Symp.*, 556.
[14] Tao, W. C. et al. 2002. The effects of HMX particle size and binder stiffness on the burning mechanism and regression rate of a series of fast burning Propellants. In *Proc. 2002 JANNAF 38th Combustion Subcommittee Meeting*, Destin, FL, April 8–12.
[15] Dobratz, B., and A. Duncan. 2001. Effect of particle size in the manufacture and characterization of energetic materials. LANL unpublished data.
[16] Elban, W. L., and M. A. Chiarito. 1986. Quasi-static compaction study of coarse HMX explosive. *Powder Technology* 46: 181.
[17] Skidmore, C. B., B. W. Olinger, and B. M. Dobratz. 2000. Densities variations in cylinders and hemispherical shells of pressed plastic bonded explosives (PBX) 9501 and 9502. *23rd Aging, Compatibility and Stockpile Stewardship Conference*, Lawrence Livermore National Laboratory, Albuquerque, NM.